An Efficient Technique for Nuclei Segmentation Based on Ellipse Descriptor Analysis and Improved Seed Detection Algorithm

Hongming Xu, Cheng Lu, *Student Member, IEEE*, and Mrinal Mandal, *Senior Member, IEEE*

Abstract—In this paper, we propose an efficient method for segmenting cell nuclei in the skin histopathological images. The proposed technique consists of four modules. First, it separates the nuclei regions from the background with an adaptive threshold technique. Next, an elliptical descriptor is used to detect the isolated nuclei with elliptical shapes. This descriptor classifies the nuclei regions based on two ellipticity parameters. Nuclei clumps and nuclei with irregular shapes are then localized by an improved seed detection technique based on voting in the eroded nuclei regions. Finally, undivided nuclei regions are segmented by a marked watershed algorithm. Experimental results on 114 different image patches indicate that the proposed technique provides a superior performance in nuclei detection and segmentation.

I. INTRODUCTION

ANALYSIS of cell nuclei plays an important role in the histopathological examination and diagnosis. Application includes diagnosis of critical diseases such as breast or skin cancer [1], [2]. Most diagnoses rendered by anatomical pathologists are generally based on the microscopic analysis of haematoxylin and eosin (H&E) stained section. Anatomical pathologists, especially cytopathologists, give special attention to the analysis of nuclei size, shape, contours, and presence or absence of nucleoli and mitotic figures within nuclei [3]. The morphological features and changes of the cell nuclei in tissues have great diagnostic value for pathological examination, and act as key roles in providing support for early cancer detection and prevention.

As the pathologists typically identify the constituent cells of interest based on their personal experience, the judgments by them are subjective and sometimes lead to intra- and interobserver variability [4]. With recent advances in digital imaging and computer hardware, computer-aided analysis of histopathological slides has become important [5]. Automated analysis of histopathological images can help in making fast diagnosis and
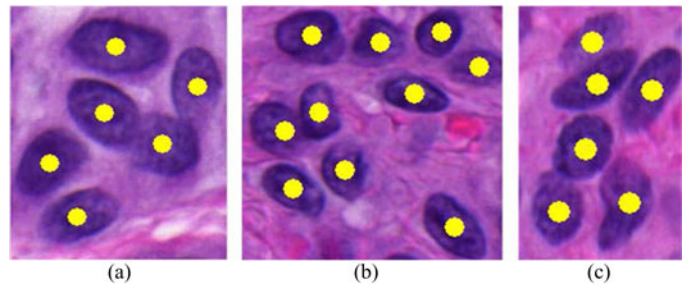

Fig. 1. Histopathological images with nuclei obtained from the digitized skin slides. The yellow seed points mark the positions and existence of the cell nuclei.

provide reliable and reproducible objective results. However, there still remains a huge challenge for a computer algorithm to perform automated analysis with high accuracy. The difficulties stem from many aspects such as the existence of nuclei clumps, blurred nuclei boundaries, and intensity variations in digitized histopathological images. Fig. 1 shows three image patches obtained from tissue blocks of skin biopsies and stained with haematoxylin and eosin (H&E). In the images, the cell nuclei are observed as dark blue whereas the intracellular material and cytoplasm are observed as bright pink. As seen, several cell nuclei touch or overlap each other; color variations exist in inter and intra images due to nonuniform absorption of the stains, stains fading, and other factors; some boundaries of the cell nuclei have been blurred. All these factors make it difficult to accurately segment the nuclei.

A major limitation of the traditional segmentation techniques such as histogram based [6] or threshold based [7] techniques is the under-segmentation of the clumped nuclei. The failure to separate the nuclei during quantitative histopathological image analysis may degrade the diagnosis performance. In order to address this, researchers have proposed a few techniques. The watershed algorithm is widely used for image segmentation due to its advantages of simplicity, speed, and absence of adjustable parameters [8]. However, the watershed algorithm usually gives rise to over-segmentation because of many local minima or under-segmentation for heavily overlapping nuclei. To overcome the problems of the classical watershed, Yang *et al.* [9] used a marker-controlled watershed algorithm to segment clustered nuclei which extracted the markers using condition erosion. However, this technique is sensitive to nuclei shape, size, and the predefined thresholds for erosion. Cheng *et al.* [10] presented a method to extract markers using an adaptive H-minima transform, and a novel marking function for
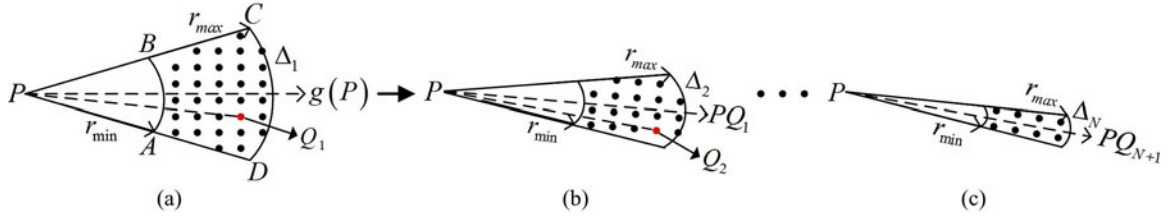
Fig. 2. Illustration of one pixel voting for the MPV algorithm [15]: (a)–(c) Shrinking cone-shape voting area with the voting direction towards the point with highest votes. Note that the point Q_i $(i = 1, 2, \ldots, N + 1)$ get the highest votes in the voting area. The angles Δ_i $(i = 1, 2, \ldots, N)$ for the cone-shape voting area is iteratively made smaller.

watershed algorithm. This method applies the same parameters directly related to the h-value to clustered nuclei in an image regardless of the nuclei shape and size. Thus, it is difficult to generate a one-to-one correspondence between the markers and nuclei. Jung *et al.* [11] further formulated the marker extraction by H-minima transform as an optimization problem and adjusted nuclei contours by the parameterized ellipsoidal models. However, this technique assumes that the nucleus has an elliptical shape, which is not always true. This can be illustrated by the fact that the 2-D nuclei images may be obtained by partial imaging or at odd angles [12]. Also note that if the maximum depth in the distance map is not located at the region around the nucleus center, both adaptive and optimal selection of h-value will not result in accurate nuclei detection and segmentation.

A few other promising methods have been proposed to perform segmentation of touching cells or nuclei. Schmitt *et al.* [13] proposed a technique for splitting cell clumps by using morphological multiscale decomposition with scalable templates and a morphological structuring element. Al-Kofaha *et al.* [12] proposed to detect nuclei markers using the multiscale Laplacian-of-Gaussian filtering and cluster nuclei regions based on the detected seeds. Although these methods have been reported to provide a good performance, the performance is overly sensitive to the predefined parameters related to nuclei size and shape. Wang *et al.* [14] presented a concavity based approach which first conducts shape classification, and then identifies a pair of splitting points and connects them by the weighted shortest path. This technique is limited to the objects with convex shapes and heavily relies on the training process for shape classification. Parvin *et al.* [15] proposed a multi-pass voting (MPV) algorithm for inferring cell or nuclei centers, which applies the refined and reoriented kernels for the voting area and considers the pixels with votes larger than the threshold as the detected seeds. Qi *et al.* [16] developed a single-pass voting (SPV) algorithm based on the work in [15], which detects cell seeds using mean shift clustering algorithm and applies the repulsive level set model [17] to segment clustered cells. Lu *et al.* [3] proposed an adaptive threshold selection method for nuclei segmentation in cutaneous histopathological images. This method first applies the hybrid morphological reconstruction technique to enhance the image, and then adaptively selects the threshold for a local region to conduct nuclei segmentation. Although the technique separates isolated nuclei or partially touching nuclei efficiently, it fails to separate highly overlapping nuclei. Plissiti and Nikou [18] presented a spatially adaptive physical model for overlapping nuclei segmentation that represents the nucleus

shape by the vibrations of a spring mass system and obtains elastic 2-D boundary by a closed chain topology of virtual masses. This technique only works automatically for the images with a known number of nuclei.

Although there have been a number of approaches proposed for automatic cell nuclei segmentation, the difficulties for most of them are often due to the fact that the number and locations of cell nuclei are not known. In this paper, we propose an efficient technique for detecting and segmenting nuclei in cutaneous histopathological images. The proposed technique detects the isolated nuclei by using the ellipse descriptor analysis, and segments nuclei clumps by using the marked watershed based on an improved seed detection algorithm. The organization of this paper is as follows. Section II provides a brief review of the background work. Section III describes the proposed technique in detail, followed by performance evaluations in Section IV. The conclusions are presented in Section V.

II. REVIEW OF BACKGROUND WORK

In this section, we present a brief review of three selected state-of-the-art techniques that are closely related to our proposed technique.

In our previous work, we proposed a local optimal threshold technique [3] for nuclei segmentation in skin histopathological images. This technique first applies the hybrid morphological reconstruction operations to reduce noise and intensity variations within nuclei regions. The nuclei shape and size are then incorporated as domain specific knowledge to select local optimal threshold for nuclei segmentation. The technique provides a good performance on images with mostly isolated nuclei, e.g., images obtained in the skin epidermis area. However, if the images have a large number of overlapping nuclei, e.g., images obtained in the skin dermis area, the segmentation performance degrades.

Parvin *et al.* [15] proposed an MPV algorithm for detecting cell or nuclei centers in microscopic images. The MPV algorithm determines a cone-shape voting area in the gradient direction of high gradient pixels [see Fig. 2(a)]. The parameters $r_{\min}$ and $r_{\max}$ are estimated based on the prior knowledge of the average nuclei size. All pixels within the area ABCD get a vote weighted by the following Gaussian kernel centered at P:

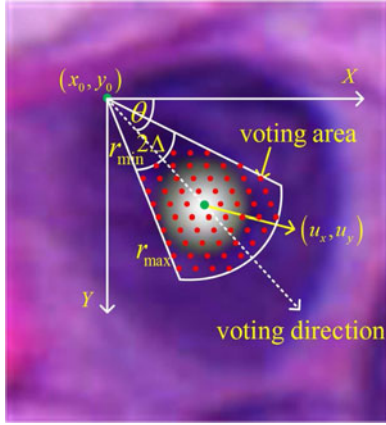$$g(x, y) = \frac{1}{\sqrt{2\pi}\sigma} e^{\frac{-(x^2 + y^2)}{2\sigma^2}} \tag{1}$$

Fig. 3. Illustration of one pixel voting for the SPV algorithm [16].

Fig. 4. Schematic of the proposed technique.

where (x, y) is an image point. For the area $ABCD$, the weight is highest for pixels on the arc AB, and smallest for pixels on the arc CD. In the second-pass voting, the angle Δ is made smaller (i.e., $\Delta_2 < \Delta_1$), and the voting direction for a pixel is aligned towards the closest pixel cluster with highest votes [see Fig. 2(b), (c)]. The subsequent passes are executed in a similar manner. When all N iterations are carried out, the pixels with votes larger than the threshold are considered as seeds.

Qi *et al.* [16] proposed an SPV algorithm with a new Gaussian kernel to improve the seed detection performance of the MPV algorithm. Here, the Gaussian kernel $g(x, y, u_x, u_y, \sigma)$ centered at the point (u_x, u_y) as defined below is applied on the cone-shape voting area (see Fig. 3):

$$g\left(x, y, u_x, u_y, \sigma\right) = \frac{1}{2\pi\sigma^2} \exp\left(-\frac{(x - u_x)^2 + (y - u_y)^2}{2\sigma^2}\right) \tag{2}$$

where $u_x = x_0 + r\cos\theta$, $u_y = y_0 + r\sin\theta$, and $r = \frac{(r_{\min} + r_{\max})}{2}$. The modes of the vote image are detected using the mean shift clustering [19] after the voting. The Gaussian kernel in (2) amplifies the votes around the center of the voting area and is able to avoid creating false seeds in the overlapping regions. The SPV algorithm reduces the computational complexity significantly. After detecting the cell seeds, cell segmentation is conducted using a level set algorithm, where the detected seeds are used as the initialization of the repulsive level set model [17]. The contour of each cell is obtained by evolving the level set function. Although the SPV algorithm [16] provides a good performance in cells or nuclei seed detection, there still exist two limitations. First, selecting the pixels with high gradient magnitude as the voting points may generate false seeds. This usually happens when there exist inter- and intra-intensity variations in the background and nuclei regions, and a fixed threshold is used for the entire image database. Second, generation of the cone-shape voting area for voting points (i.e., high gradient points) by searching pixels from the whole image is a time consuming process. This is most evident when we deal with a large image.

Based on the above analysis, we propose here an efficient technique for the segmentation of both isolated nuclei and nuclei clumps. The propose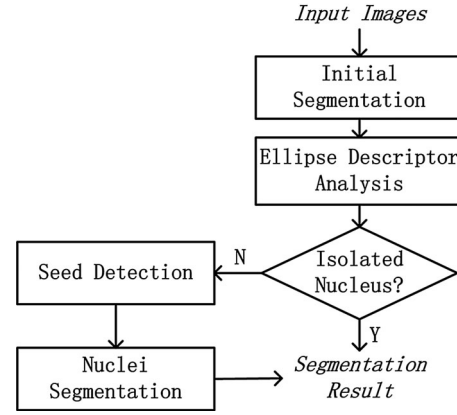d technique is implemented based on an initial segmentation of nuclei regions, which is followed by a fine segmentation of nuclei clumps. The isolated nuclei obtained after initial segmentation are detected by an ellipse descriptor analysis. Nuclei clumps are segmented by the marked watershed with an improved seed detection algorithm. Overall, the limitations of our previous work [3] and the SPV algorithm [16] are addressed.

III. THE PROPOSED TECHNIQUE

The schematic of the proposed technique for cell nuclei segmentation is shown in Fig. 4. It is observed that there are four modules. In the first module, an initial segmentation of cell nuclei regions is performed using an adaptive thresholding technique. In the second module, an elliptical descriptor is used to filter the isolated nuclei with elliptical shapes in the initially segmented binary image. This descriptor classifies the isolated nuclei according to two ellipticity parameters of the nuclei region. In the third module, an efficient voting algorithm is applied to detect seeds of nuclei clumps and the nuclei with irregular shapes. In the fourth module, the undivided nuclei are segmented by the marked watershed algorithm with the contours adjusted by the ellipsoidal modeling. The details of four modules are now presented in the following.

A. Initial Segmentation

Due to the staining imperfection and variation, the pixel intensity in nuclei regions is not homogenous. Blurred nuclei boundaries and noisy pixels in the background are usually observed. The traditional low level segmentation methods (i.e., histogram based method [6]) generally fail to precisely segment the cell nuclei regions from the background pixels. After comparing several segmentation techniques including Otsu's method [7], active contour model [20], [21], and graph cut [22], an adaptive threshold technique [3] is adopted for the initial segmentation of cell nuclei in this paper.

The principal steps for initial segmentation by the adaptive threshold technique are:
1) Enhance the image using the hybrid gray-scale morphological reconstructions module. In this module, the R channel of the original RGB image is used as
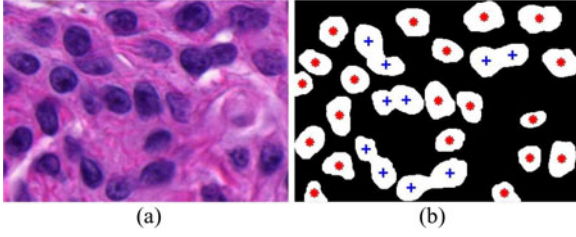
Fig. 5.   Example of the initial segmentation. (a) The original image. (b) The segmentation result. Note that ∗ indicate the isolated nuclei, whereas + indicate the touching nuclei.
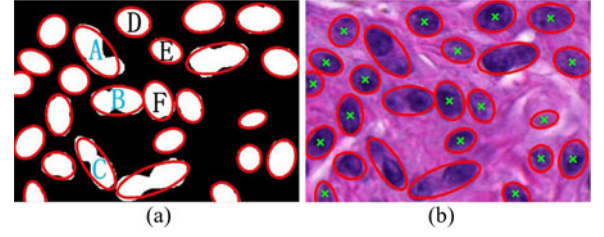

Fig. 6.   Elliptical modeling for each connected region. (a) The ellipse model constructed from Fig. 5(b). (b) The ellipse model superimposed on the original image. Note that the × in (b) mark the ellipse centers for the detected isolated nuclei.

the input. Opening-by-Reconstruction and Closing-by-Reconstruction are consecutively applied to reduce the impact of undesirable variations in the image and to make the nuclei region homogenous.

2) Apply the adaptive thresholding [23] on the enhanced image. For each pixel in the enhanced image, a threshold is calculated as the mean intensity of the local neighborhood (e.g., 60×60). Since the intensity of nuclei regions is lower than the background, a pixel value below the threshold is set to the foreground value (represented by 1), and a pixel value above the threshold is set to the background value (represented by 0).

3) Enhance the segmented result by a series of morphological operations. The holes within the segmented regions are filled by performing the morphological reconstruction. The small isolated regions, unlikely to be the nuclei, are removed by conducting an opening operation with a disc structuring element. Fig. 5(a) shows an original image, and Fig. 5(b) shows the segmentation result.

B. Ellipse Descriptor Analysis

It is observed in Fig. 5(b) that initial segmentation results in both isolated nuclei and nuclei clumps. Assume that the segmented regions in Fig. 5(b) are denoted as $\{N_p\}_{p=1...Z}$, where Z is the total number of regions. In this module, we classify $\{N_p\}_{p=1...Z}$ as the isolated nuclei or the nuclei clump. Based on the observation that the isolated nuclei in skin histopathological images typically have elliptical boundaries, most isolated nuclei can be detected by using an elliptical model. To build the elliptical model for each region in $\{N_p\}_{p=1...Z}$, we first calculate the gradient image of the initial segmentation result, and then obtain the boundary points by selecting positions with nonzero gradient magnitudes. Using the obtained boundary points, each region in $\{N_p\}_{p=1...Z}$ is now mathematically described by an elliptical model. Let (x, y) be a 2-D boundary point of a connected region. The ellipse is modeled by the following second-order polynomial [24]:

$$E(\overline{a}, \overline{x}) = \overline{a} \cdot \overline{x} = ax^2 + bxy + cy^2 + dx + ey + f = 0 \quad (3)$$

where $\overline{a} = [a\ b\ c\ d\ e\ f]^T$ denotes the ellipse coefficients, $\overline{x} = [x^2\ xy\ y^2\ x\ y\ 1]^T$, and $E(\overline{a}, \overline{x})$ is the algebraic distance from the point (x, y) to the conic $E(\overline{a}, \overline{x}) = 0$. The optimal ellipse fitting the nuclei shape is generated by minimizing the

TABLE I
THE VALUES OF ELLIPTICITY PARAMETERS FOR SEVERAL SELECTED CANDIDATE REGIONS SHOWN IN FIG. 6(A)

Ellipticity Parameters	A	B	C	D	E	F
e_1	0.87	0.88	0.86	0.95	0.97	0.94
e_2	0.26	0.21	0.29	0.09	0.07	0.10

sum of squared algebraic distances between the ellipse and the 2-D boundary points of the connected region [24].

After generating the elliptical model for each region N_p, the ellipticity evaluation is performed by comparing the region of N_p and the corresponding ellipse. Let R_n be the set of pixels in N_p (i.e., the nucleus or the nuclei clump), and R_e be the set of pixels in the elliptical region. We use the following two parameters e_1 and e_2 to measure the ellipticity of a region:

$$e_1 = \frac{|R_n \cap R_e|}{|R_e|} \quad (4)$$

$$e_2 = \frac{|R_n \Delta R_e|}{|R_e|} \quad (5)$$

where $|\cdot|$ is the cardinality of the pixels set, $\cap$ is the intersection operation, and Δ is the symmetric difference operation. Intuitively, the higher value of the ellipticity parameter e_1 and the lower value of the ellipticity parameter e_2 represent a closer match to an elliptical shape. Thus, the candidate region with high value of e_1 and low value of e_2 is more likely to be a single nucleus. On the other hand, a region with lower value of e_1 but higher value of e_2 is expected to be a nuclei clump or a nucleus with the irregular shape.

An example of the ellipse descriptor analysis is shown in Fig. 6. Fig. 6(a) shows the ellipses obtained by fitting the boundary points of the binary image shown in Fig. 5(b). The markers A, B, C indicate the three regions formed by the touching nuclei, while the markers D, E, F indicate three typically isolated cell nuclei with elliptical shapes. Fig. 6(b) also shows the constructed ellipses superimposed on the original image. The values of the ellipticity parameters e_1 and e_2 for the candidate regions $A - F$ are shown in Table I. It is observed that the regions of the single nucleus D, E, F have high values of e_1 (close to 1.0) and low values of e_2 (close to 0.0). In contrast, the candidate regions A, B, C are separately formed by two touching nuclei,
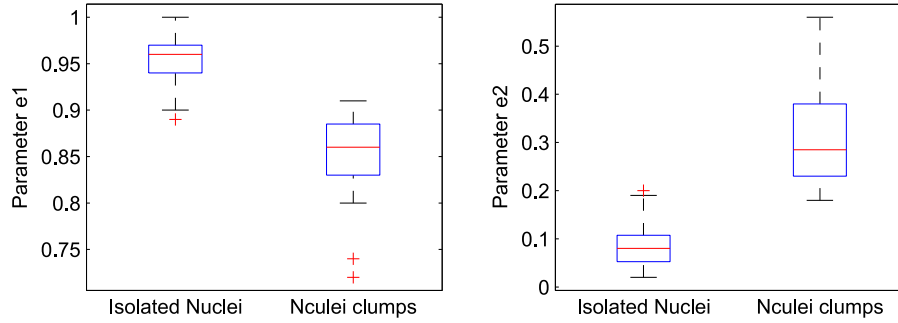
Fig. 7. Variations of ellipticity parameters $e1$ and $e2$ for isolated nuclei and nuclei clumps.

and they have relatively lower values of e_1 (around $0.8 \sim 0.9$) but higher values of e_2 (around $0.2 \sim 0.3$). Therefore, the single nucleus with elliptical shape is detected by the aforementioned two defined parameters. A segmented region N_p is determined as a single nucleus if both of the following two conditions are satisfied:

$$e_1 \geq \tau_1 \tag{6}$$

$$e_2 \leq \tau_2 \tag{7}$$

where τ_1 and τ_2 are the predefined thresholds. In order to calculate the parameters τ_1 and τ_2, 170 nuclei regions in 15 randomly selected image patches are manually labeled, and the values of e_1 and e_2 for each region are calculated. Fig. 7 shows the box plots of ellipticity parameters for isolated nuclei and nuclei clumps in 170 nuclei regions. It is observed that isolated nuclei on average have a high value of e_1 (0.96) and a low value of e_2 (0.07), whereas nuclei clumps have a lower value of e_1 (0.85) and a higher value of e_2 (0.30). The isolated nuclei with elliptical shapes can be separated from nuclei clumps by thresholding the two ellipticity parameters. In this paper, the values of τ_1 and τ_2 are calculated as follows:

$$\tau_1 = \frac{\overline{e_{1N}} + \overline{e_{1C}}}{2} \tag{8}$$

$$\tau_2 = \frac{\overline{e_{2N}} + \overline{e_{2C}}}{2} \tag{9}$$

where $\overline{e_{1N}}$ and $\overline{e_{1C}}$ are the average values of e_1 for isolated nuclei and nuclei clumps, $\overline{e_{2N}}$ and $\overline{e_{2C}}$ are the average values of e_2 for isolated nuclei and nuclei clumps, respectively. Note that the nuclei regions (i.e., single nucleus) that satisfies the above two conditions in Fig 6(b) are marked with crosses at the ellipse centers. The subsequent sections are not applied on these regions, while the other regions [i.e., nuclei clumps A, B, C in Fig 6(a)] are segmented by the marked watershed algorithm.

C. Seed Detection

After the ellipse descriptor analysis, most isolated cell nuclei with elliptical shapes have been detected. To segment the remaining cell nuclei regions, for example the regions $A - C$ shown in Fig 6(a), the marked watershed algorithm is applied. In this module, we present a voting algorithm for detecting seeds
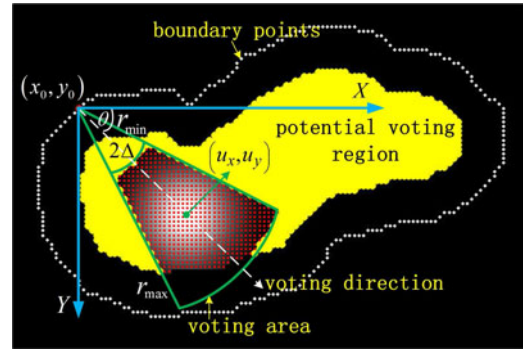

Fig. 8. Cone-shape voting area with a Gaussian kernel superimposed on the nuclei region after the erosion operation.

of nuclei clump and nuclei with irregular shapes. The detected seeds are used as the markers for watershed algorithm.

Assume that the nuclei regions, which are waiting for seed detection, are denoted as $\{N_i\}_{i=1...K}$, where K is the number of connected regions. The regions $\{N_i\}_{i=1...K}$ are first labeled via an eight-connected criterion [23], and then each region is put into a binary image which has the same size as the original image. Let $I_i(x, y)$ be a binary image which contains a region N_i. The boundary points set $T_i(x, y)$, the corresponding image gradient $\nabla T_i(x, y)$ and the gradient magnitude $\|\nabla T_i(x, y)\|$ are computed subsequently. Since the nuclei regions in the binary image $I_i(x, y)$ are the white foreground, the voting direction for a boundary point is defined as the positive gradient direction $\frac{\nabla T(x,y)}{\|\nabla T(x,y)\|} = (\cos(\theta(x, y)), \sin(\theta(x, y)))$, where θ is the angle of the gradient direction with respect to the horizontal direction of the image. Fig. 8 illustrates an example of voting for a boundary point (x_0, y_0). The parameters $r_{\min}, r_{\max}$, and Δ define a cone-shape voting area. The dashed contours represent the extracted boundary points. The potential voting region (e.g., the yellow region) is obtained by performing the erosion operation on the original nuclei region. The points (e.g., red points) in both the cone-shape voting area and the potential voting region get the votes weighed by the Gaussian kernel centered at the point (u_x, u_y). The Gaussian kernel is defined in (2).

Note that prior to voting towards the gradient direction of boundary points, the erosion operation is applied to shrink the nuclei region N_i. The structuring element S for the erosion
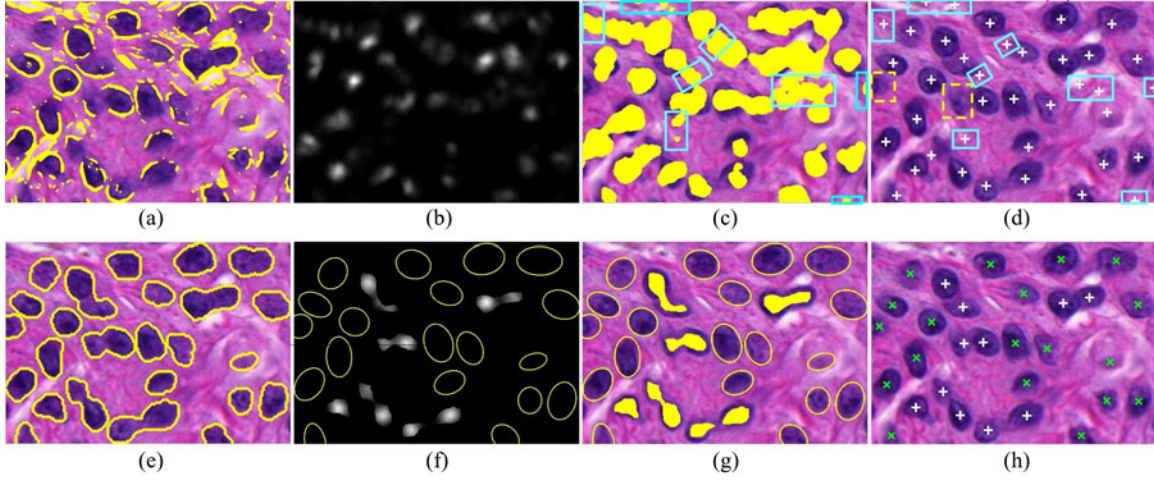
Fig. 9. Comparison of the seed detection performance by the SPV technique [16] (shown in the first row) and the proposed technique (shown in the second row). (a) Image with extracted voting points (i.e., high gradient points). (b) Final vote image. (c) Image with vote points. (d) Image with detected seeds by the SPV technique. (e) Image with extracted voting points (i.e., nuclei boundary points). (f) Final vote image with ellipse contours of isolated nuclei. (g) Image with vote points and ellipse contours of isolated nuclei. (h) Image with detected seeds by the proposed technique. Note that the votes outside nuclei regions in (c) are marked with solid rectangles. The false seeds and nuclei without seeds in (d) are marked with solid and dashed rectangles respectively.

operation is defined as follows:

$$
S = \begin{bmatrix}
0 & 0 & 0 & 1 & 0 & 0 & 0 \\
0 & 1 & 1 & 1 & 1 & 1 & 0 \\
0 & 1 & 1 & 1 & 1 & 1 & 0 \\
1 & 1 & 1 & 1 & 1 & 1 & 1 \\
0 & 1 & 1 & 1 & 1 & 1 & 0 \\
0 & 1 & 1 & 1 & 1 & 1 & 0 \\
0 & 0 & 0 & 1 & 0 & 0 & 0
\end{bmatrix}. \tag{10}
$$

The disk-shaped structuring element with radius of three pixels is empirically applied such that the erosion operation is able to retain the actual shape when reducing the size of nuclei regions. In this paper, the size of each region in $\{N_i\}_{i=1...K}$ is reduced by at least half. But note that if the erosion operation has generated the isolated small region (i.e., ≤ 100 pixels), it should stop continually eroding the obtained small region to avoid the small nucleus disappearing. The erosion operation is performed for two reasons. First, the nuclei centers are far away from nuclei boundaries, and hence there is no need to vote for pixels near the nuclei edges. Although the cone-shape voting area used in [16] could theoretically avoid the votes approaching to nuclei edges, in practice the pixels near nuclei boundaries or even outside nuclei regions may still get votes [see Fig. 9(c) where the votes outside nuclei regions are marked with solid rectangles]. This is because nuclei shape and size vary greatly from each other, but the fixed parameters $r_{\min}$ and $r_{\max}$ are used for all nuclei in an image, and the gradient direction does not always point to nuclei centers. Second, the erosion operation contributes to reducing the time requirement of the voting algorithm by reducing the number of calculations, since the potential voting region (i.e., the original nuclei region) has been shrunk and there are fewer pixels that can get votes. For example, in Fig. 8, only the pixels in the eroded nuclei region (i.e., yellow region) may get votes.

Now let $V_i(x, y)$ be the vote image for the binary image I_i, and have the same size as the original image. All pixels in

$V_i(x, y)$ are first initialized as zeros, and then updated as:

$$
\begin{aligned}
V_i(x, y) = {} & V_i(x, y) \\
& + \sum_{(x,y) \in A(m,n)} \|\nabla T_i(m, n)\| \, g(x, y, u_m, u_n, \sigma)
\end{aligned} \tag{11}
$$

where (m, n) represents a nuclei edge point, $A(m, n)$ is the voting area for the point (m, n), $g(x, y, u_m, u_n, \sigma)$ is the Gaussian kernel centered at (u_m, u_n). The final vote image V is the sum of all images V_i. Assume the value for a point $(x, y) \in V$ be n, we interpret that the point (x, y) is observed n times. Using the positions of the points in V as the two dimensional feature space, the nuclei seeds are computed by executing mean shift clustering algorithm [19]. The detailed process of the proposed voting algorithm is shown in Algorithm 1.

Algorithm 1 The proposed voting algorithm

Input: Candidate nuclei regions set $\{N_i\}_{i=1...K}$.
Initialization: $r_{\min} = 0.4d$, $r_{\max} = 1.5d$, $\Delta = \frac{\pi}{6}$, $\sigma = 7$ and $r_{bw} = 0.6d$, where d is the estimated average radius of the nuclei in the image, r_{bw} is the bandwidth of the mean shift algorithm.
for each region N_i **do**
  Compute boundary points set $T_i(x, y)$, image gradient $\nabla T_i(x, y)$, gradient magnitude $\|\nabla T_i(x, y)\|$ and gradient directions $\frac{\nabla T(x,y)}{\|\nabla T(x,y)\|}$.
  Perform erosion operation on nuclei region N_i.
  Initialize the vote image V_i, and conduct the single-path voting using Eq. 11.
end for
Sum all the vote images V_i and run the mean shift clustering algorithm to localize nuclei seeds.
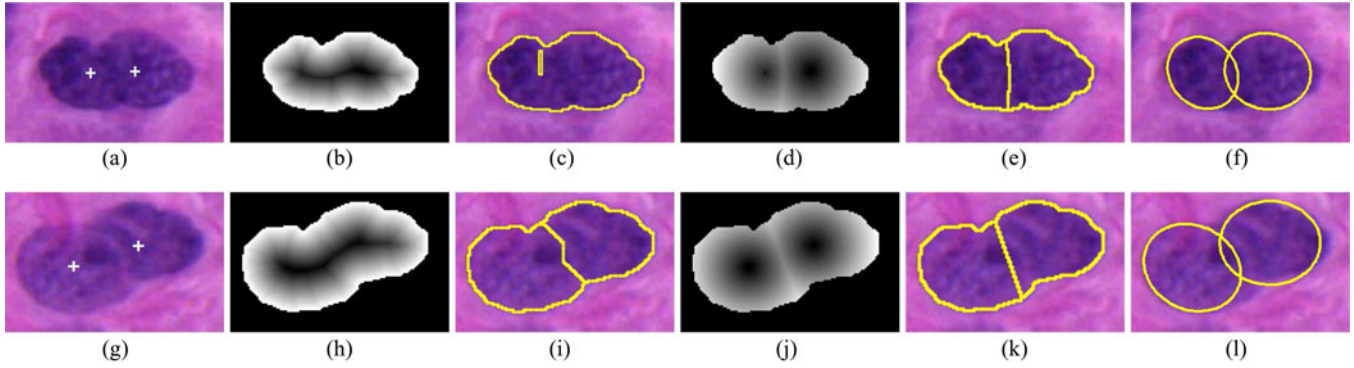**Output:** The nuclei seeds for regions $\{N_i\}_{i=1...K}$.

Fig. 10. Comparison of watershed segmentation using two different marking functions. (a) and (g) Original images with detected seeds. (b) and (h) Inner distance maps. (c) and (i) Segmentation results using inner distance maps as marking function. (d) and (j) New distance maps. (e) and (k) Segmentation results using new distance maps as marking function. (f) and (l) Contours adjusted by the elliptical model. Note that under-segmentation and the jagged watershed line are observed in (c) and (i), respectively. The valleys connecting the regional minima shown in (b) and (h) are broken in (d) and (j).

Our work of seed detection is extended from [16], but it differs in several significant aspects: (1) The original color image is transformed into a binary one using initial segmentation techniques discussed in Section A. The boundary points of the regions $\{N_i\}_{i=1\ldots K}$ are used for voting. This step is critical which eliminates the votes from other high gradient pixels in nuclei regions or the background. (2) Most isolated cell nuclei with elliptical shapes are detected by the ellipse descriptor analysis discussed in Section B, which avoids unnecessary seed detection and segmentation for them. (3) Instead of searching the voting areas from the whole image, we first conduct the erosion operation on each nuclei region N_i, and then select the voting areas from the eroded nuclei region. This step enables the votes to mainly concentrate on the regions around nuclei centers and completely avoids the votes outside the nuclei regions to generate false seeds. More importantly, selection of the voting areas from the eroded binary nuclei regions rather than from the whole image markedly reduces the computational complexity of the voting algorithm.

In Fig. 9, we compare the entire process of the seed detection between using the SPV algorithm [16] and the proposed voting algorithm. The first row of Fig. 9 separately shows the extracted voting points (i.e., high gradient points), the vote image, the image with vote points, and the image with nuclei seeds generated by the SPV algorithm, while the second row shows the comparison results using the proposed technique. As seen in Fig. 9(a), a large number of high gradient pixels in the background are mistakenly considered as the voting points. The incorrect voting points in the background vote for the pixels outside nuclei regions, which are enclosed by the solid rectangles in Fig. 9(c). In Fig. 9(d), the false seeds obtained by clustering vote points outside nuclei regions are enclosed by solid rectangles, and the nuclei without seeds due to the blurred edges with low gradient points are enclosed by dashed rectangles. In Fig. 9(h), the crosses × indicate the centers obtained by the ellipse descriptor analysis, whereas the crosses + represent the nuclei seeds obtained by the proposed voting algorithm. For more examples of seed detection results, please refer to the seed detection performance in Section IV.

D. Nuclei Segmentation

Using the detected seeds obtained from section C as the markers, the segmentation of nuclei clumps can be efficiently performed by the marked watershed algorithm. However, the segmentation by watershed algorithm not only depends on the markers but also depends on the marking function [10]. For separation of partially touching nuclei, the watershed algorithm using the classical marking function [8] works well, but it fails to separate highly overlapping nuclei due to the valley connecting the regional minima in the inverse inner distance map [see Fig. 10(b), (c)]. Further, the jagged watershed lines [see Fig. 10(i)] generated by the classical marking function are usually not desirable [10]. To address these two limitations, we propose a new marking function for the watershed algorithm, which is calculated based on the inner distance map and the distances between nuclei seeds and pixels in nuclei regions.

Let $I_i(x, y)$ be a binary image containing a nuclei region N_i and $C = (C_1, C_2, \ldots, C_K)$ be the detected nuclei seeds in this region. The distance transform for the new marking function is calculated as follows:

1) Calculate the Euclidean distance $D_j(x', y')$ between the jth seed C_j and the pixel (x', y') for all $1 \leq j \leq K$, where $(x', y') \in N_i$.
2) Calculate the inner distance transform $d_i(x', y')$ for the pixel (x', y'):

$$d_i(x', y') = \inf_{(x,y) \in B_i} \sqrt{(x' - x)^2 + (y' - y)^2} \quad (12)$$

where B_i is the background region in I_i.
3) Obtain the new depth value $f_i(x', y')$ for the pixel (x', y'):

$$f_i(x', y') = \min_j \{D_j(x', y') - d_i(C_j)\} \quad (13)$$

where $d_i(C_j)$ is the depth value for the nuclei seed C_j $(1 \leq j \leq K)$ in d_i.

The distance map f_i defined in (13) is similar to that proposed in [10], which is capable of breaking the valley connecting the regional minima caused by the inner distance transform and avoiding the jagged watershed lines of segmented nuclei.

TABLE II
COMPARISON OF SEED DETECTION PERFORMANCE BETWEEN SPV ALGORITHM AND PROPOSED TECHNIQUE

Techniques	Database-1				Database-2			
	N_P	N_{DS}	$PRE(\%)$	$SEN(\%)$	N_P	N_{DS}	$PRE(\%)$	$SEN(\%)$
SPV [16]	872	922	64.32	68.00	1271	1321	74.94	77.89
Proposed	**872**	**935**	**85.99**	**92.20**	**1271**	**1267**	**94.40**	**93.71**

Fig. 10 shows two examples of nuclei segmentation by watershed algorithm using two different marking functions. The under-segmentation for highly overlapping nuclei is observed in Fig. 10(c), which is obtained by using the classical marking function in [8] with the inner distance transform [see Fig. 10(b)]. In contrast, the watershed algorithm using the proposed marking function separates the overlapping nuclei as desired [see Fig. 10(e)]. The jaggedness of the watershed line generated by the classical marking function is observed in Fig. 10(i), whereas the smooth watershed line is obtained by using the proposed marking function [see Fig. 10(k)]. The jagged contours of nuclei generated by watershed algorithm can be further alleviated by the parameterized ellipsoidal models [11]. Assume that the elliptical models for nuclei are mutually independent and can be overlapped, each model can be generated by using the direct least square fitting algorithm [24] based on the boundary points of the nucleus region. Fig. 10(f), (l) separately show nuclei segmentation with the smooth contours obtained by the parameterized ellipsoidal models.

IV. PERFORMANCE EVALUATIONS

We have evaluated the proposed technique on two databases containing 114 different cutaneous histopathological image patches with more than 2000 nuclei. The first database consists of images of skin epidermis mainly with isolated nuclei, while the second database consists of images of skin dermis mainly with nuclei clumps. The histological sections used for image acquisition were prepared from formalin-fixed paraffin-embedded tissue blocks of skin biopsies and stained with haematoxylin and eosin (H&E) by automated stainer. The test images on average have the size of 500×500 pixels (pixel resolution: $0.23\ \mu$m/pixel) and were captured under 40X magnification on Carl Zeiss MIRAX MIDI Scanning system (Carl Zeiss Inc., Germany). The major axis of a nucleus generally ranges between 40 and 70 pixels. In this section, we present the nuclei detection and segmentation performance of the proposed technique.

A. Seed Detection Performance

To evaluate the performance of the developed seed detection technique, the nuclei locations are manually labeled using an interactive computer program (based on MATLAB). The marker indicating a nucleus is recorded by the user mouse clicking operation during the manual labeling procedure. Three examples of image patches with nuclei markers have been shown in Fig. 1 in which the bright yellow dots indicate the manually labeled markers for the presence of nuclei. These manually labeled nuclei markers are taken as the ground truth annotation for the nuclei detection performance evaluation. A nucleus seed is considered as correctly detected if its location is within a range of 10 pixels of the manually labeled nucleus location.

Let N_P, N_{DS}, and N_{TP} denote the numbers of the ground truth seeds, the detected seeds, and the true positives (i.e., correctly detected seeds) respectively. The performance is evaluated with respect to the precision (PRE) and the sensitivity (SEN) which are defined as follows:

$$\text{PRE} = \frac{N_{TP}}{N_{DS}} \times 100\% \tag{14}$$

$$\text{SEN} = \frac{N_{TP}}{N_P} \times 100\%. \tag{15}$$

The seed detection performance of the proposed voting algorithm is compared with that of the SPV algorithm [16]. For the both algorithm, the values of parameters $r_{\min}, r_{\max}$, and r_{bw} are determined by the estimated average nuclei radius in the database. These parameters are set to $r_{\min} = 10, r_{\max} = 40$, and $r_{\text{bw}} = 16$ after calculating the average radius of 170 manually selected nuclei in the training database. The parameter Δ is set as $\frac{\pi}{6}$ which is same as that in [16]. The threshold to select voting points (i.e., high gradient pixels) for the SPV algorithm is empirically set as 0.035. The proposed voting algorithm detects nuclei seeds only for nuclei clumps and nuclei with irregular shapes, whereas the SPV algorithm is implemented to detect nuclei seeds for all nuclei regions. To compare the performance of these two methods, the region centers of isolated nuclei detected by the ellipse descriptor analysis are taken as nuclei seeds. Table II shows the comparison results of two approaches tested on two databases. It is observed that the proposed technique achieves a superior precision and sensitivity in comparison to the results obtained by the SPV algorithm. The poor performance for the SPV algorithm is mainly due to the inter- and intra-intensity variations present in the test images. Simply by setting a single threshold for the whole image database, it is difficult to obtain a good detection performance. The votes outside nuclei regions could potentially generate false seeds. The nuclei with blurred edges (i.e., low gradient points) cannot get votes, and hence no seeds are detected for them.

For visual comparison, Fig. 11 shows four randomly selected examples of seed detection results from two databases. The first column shows the original images; the second column shows the images overlapped with nuclei edges obtained after the initial segmentation; the third column shows the images with nuclei seeds obtained by the ellipse descriptor analysis; and the fourth and fifth columns show the final seed detection results obtained
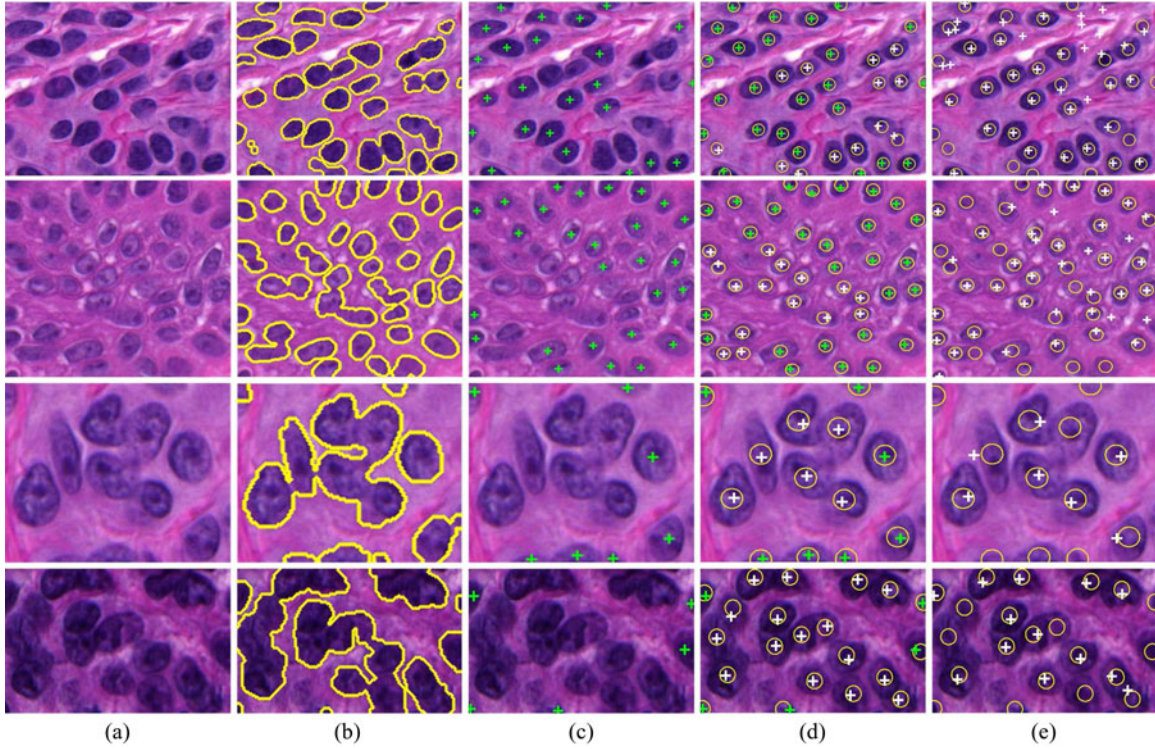
Fig. 11. Comparative seed detection results on four test images. (a) The original image patches. (b) Images with nuclei edges obtained after the initial segmentation. (c) Images with nuclei seeds obtained after the ellipse descriptor analysis. (d) Images with nuclei seeds obtained by the proposed technique. (e) Images with nuclei seeds obtained by the SPV algorithm. Note that the images in the first and second rows are selected from the database-1, while the other images are selected from the database-2. The yellow circles in the last two columns are centered at the manually labeled ground truth.

by using the proposed technique and the SPV algorithm. Note that the marked circles with radius of 10 pixels in last two columns are centered at the manually labeled nuclei positions. It is observed in the last column that the SPV algorithm generates a large number of false seeds in the background regions and misses several seeds for the nuclei with blurred boundaries, whereas the proposed algorithm provides more reliable and accurate seed detection results shown in the fourth column.

B. Segmentation Performance

To illustrate the efficacy of nuclei segmentation, the performance of the proposed technique is compared with those of various watershed-based segmentation techniques including classical watershed [8], condition erosion [9], shape marker [10], and marker optimization [11]. The results are further compared with ones from local optimal threshold [3] and SPV+level set [16]. All the parameters of these existing methods were selected such that the best segmentation performance is achieved on our databases. Let $N_{\mathrm{CS}}, N_{\mathrm{OS}}$, and N_{US} be the numbers of the correct segmentation, over-segmentation, and under-segmentation. The overall performance is evaluated using three metrics: (1) the correct segmentation rate (CSR); (2) the over-segmentation rate (OSR); (3) the under-segmentation rate (USR) which are defined as:

$$\mathrm{CSR} = \frac{N_{\mathrm{CS}}}{N_P} \times 100\% \tag{16}$$

$$\mathrm{OSR} = \frac{N_{\mathrm{OS}}}{N_P} \times 100\% \tag{17}$$

$$\mathrm{USR} = \frac{N_{\mathrm{US}}}{N_P} \times 100\% \tag{18}$$

where N_p is the number of manually labeled ground truth.

In order to evaluate the accuracy of segmented contours, the contours of 180 randomly selected nuclei from our two databases are manually labeled. The pixel-wise comparison of nuclei contours between automatic and manual segmentations is evaluated by the mean absolute distance (MAD) metric which is defined as follows:

$$\mathrm{MAD}\left(C^{\mathrm{GT}}, C^{\mathrm{SEG}}\right) = \frac{1}{N} \sum_{i=1}^{N} \left[\min \left\| C_i^{\mathrm{GT}} - C_j^{\mathrm{SEG}} \right\| \right] \tag{19}$$

where C^{GT} and C^{SEG} are the contours of manually segmented regions and automatic segmented regions, respectively, C_i^{GT} and C_j^{SEG} represent the ith pixel and the jth pixel on the contours of manually segmented regions and automatic segmented regions, respectively, and N is the total number of pixels on the contour of a manually segmented region.

The quantitative comparison of segmentation results with different methods are presented in Table III. It is observed that 92.18% and 93.15% of the cell nuclei in two databases are correctly segmented by the proposed technique, which performs relatively better than the marker optimization [11] and the shape marker [10]. Both these methods detect nuclei markers by using

TABLE III
COMPARISON OF NUCLEI SEGMENTATION PERFORMANCE BY PROPOSED TECHNIQUE AND SEVERAL EXISTING METHODS

Techniques	Database-1					Database-2				
	$CSR(\%)$	$OSR(\%)$	$USR(\%)$	MAD	$\bar{t}(s)$	$CSR(\%)$	$OSR(\%)$	$USR(\%)$	MAD	$\bar{t}(s)$
Classical Watershed [8]	47.25	49.77	2.98	4.81	0.71	49.65	49.41	0.94	3.89	0.36
Optimal Threshold [3]	88.41	6.31	5.28	2.20	7.18	76.24	6.22	17.54	3.51	3.59
SPV+Level Set [16]	67.32	5.41	27.27	2.09	156.7	77.73	4.80	17.47	2.08	86.8
Condition Erosion [9]	84.75	7.80	7.45	1.85	1.38	79.62	8.50	11.88	2.03	0.83
Shape Marker [10]	86.81	5.85	7.34	1.85	8.37	85.92	3.30	10.78	2.40	5.73
Marker Optimization [11]	88.07	5.05	6.88	1.83	6.59	87.88	1.73	10.39	2.19	2.02
Proposed Technique	**92.18**	**2.43**	**5.39**	**1.71**	**4.40**	**93.15**	**0.79**	**6.06**	**1.53**	**2.10**

the H-minima transform to suppress undesired local minima. The former method [11] determines the optimal h-value based on the hypothesis that a single nucleus has an elliptical shape, but this assumption is not always true. The latter method [10] adaptively learns h-value using the same parameters for the whole image which makes it difficult to extract the nuclei markers. Since the identical erosion structures and fixed thresholds are applied for all cell nuclei regardless of their size and shapes, condition erosion [9] occasionally generates under-segmentation and over-segmentation for nuclei clumps. The poor performance of the repulsive level set [16] is mainly due to the incorrect detection of nuclei seeds by the SPV algorithm. The local optimal threshold [3] achieves a good performance in database-1 (which mainly contains isolated nuclei) but a poor performance in database-2 (which mainly contains nuclei clumps). The main reason is that this technique is capable of separating partially touching nuclei but fails to deal with overlapping or highly clustered nuclei. The performance of the classical watershed [8] is much poorer than that of the other techniques, as the classical watershed produces high over-segmentations due to many local region minima in the distance map. It is also observed that the MAD values for the proposed technique are the smallest in the two databases among all compared methods. This is mainly due to the accurate nuclei detection of the proposed technique.

Visual examples of nuclei segmentation by the proposed technique and several existing methods are shown in Fig. 12. The first column shows the original image patches; the second column shows the manually labeled nuclei contours; the columns $(c - h)$ show the segmentation results obtained by the existing methods and the last two columns show the segmentation results obtained by the proposed technique. Note that the original image patches in the first and second rows are selected from database-1, while the original image patches in the third and fourth rows are selected from database-2. As observed in Fig. 12, when cell nuclei partially touch each other, the existing methods such as in [9]–[11] are generally capable of nuclei segmentation. But when the nuclei are severely clustered together (i.e., the third and fourth rows in Fig. 12), the methods tend to generate under-segmentation and over-segmentation. This is mainly due to the incorrect markers extraction of those methods. Overall, the proposed technique provides a more precise and reliable segmentation performance compared to existing techniques. In addition, the jaggedness of nuclei contours is removed by describing the nuclei regions with elliptical shapes.

There are three parameters that play significant roles in the proposed technique. These are ellipticity thresholds τ_1, τ_2, and estimated nuclei radius d (note that the parameters $r_{\min}, r_{\max}$, and r_{bw} are determined by d as defined in Algorithm 1). The thresholds τ_1 and τ_2 are the average values of ellipticity parameters corresponding to isolated nuclei and nuclei clumps (see (8) and (9)). To evaluate the sensitivity of these two parameters, we varied τ_1 by 1% and 2%, τ_2 by 10% and 20% around the calculated values ($\tau_1 = 0.9, \tau_2 = 0.2$), respectively. The small variation of τ_1 is selected, because a large variation may generate nonpermissible τ_1 values (e.g., $\tau_1 > \overline{e_{1N}}$). Fig. 13(a) shows the CSRs of two databases with different (τ_1, τ_2) values. As observed, CSR value varies about 1.3% in database-1, and 3% in database-2. Most nuclei in database-1 are isolated, and hence threshold variations (e.g., $\tau_1 = 0.88, \tau_2 = 0.24$) have less impact on this database. To evaluate the sensitivity of the parameter d, its value is varied by 10% and 20% around the estimated optimal value ($d = 27$). Fig. 13(b) shows the CSR values of two databases with different d values. As observed, CSR value varies about 2% for two databases. From the results in Fig. 13, it can be concluded that the proposed technique is robust to the choice of parameters τ_2 and d. The performance is relatively more sensitive to τ_1, as it has strong influence on the undersegmentation and oversegmentation. Therefore, an accurate choice of the ellipticity parameters of isolated nuclei and nuclei clumps is important.

C. Computational Complexity

To evaluate the computational complexity of the proposed technique, the average run time of the proposed algorithm tested on two databases is calculated and compared with that of the existing segmentation techniques. All experiments were carried out on a 2.3-GHz Intel Core i5-3427U CPU with 4.0-GB RAM using MATLAB 7.12. The sixth and eleventh columns of Table III separately show the average run time $\bar{t}$ for each segmentation technique. As observed, the value of $\bar{t}$ for the SPV+level set is highest (156.7 s and 86.8 s, respectively) and much larger than that of the other techniques. This is primarily due to the high complexity of the SPV algorithm [16] (which takes more than 90% of the total time for the SPV+level technique). The proposed technique on average takes 4.4 and 2.1 seconds per image patch for the two databases, which are similar to the other methods but much lower than the SPV+level set.
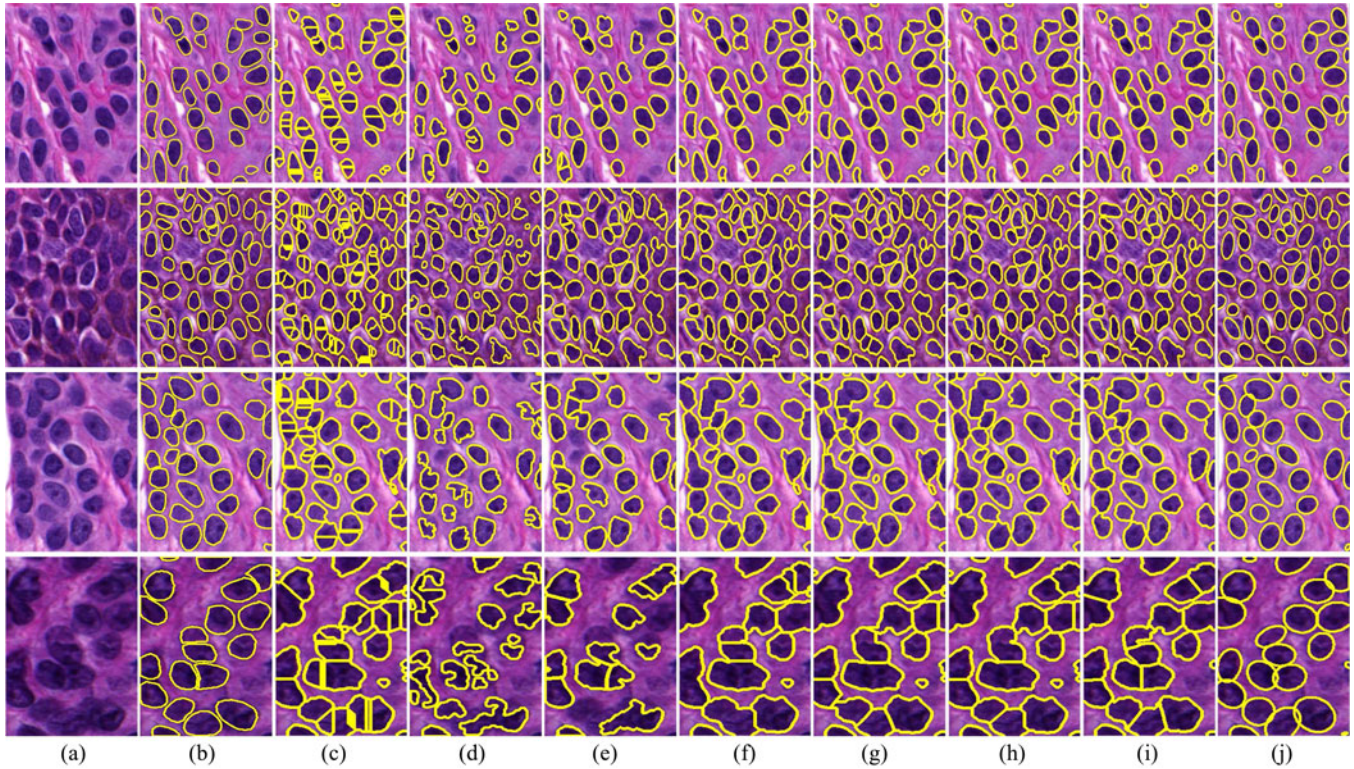
Fig. 12. Comparative segmentation results on four representative image patches. (a) The original image patches. (b) Manually labeled nuclei contours. (c) Classical watershed [8]. (d) Local optimal threshold [3]. (e) SPV+level set [16]. (f) Condition erosion [9]. (g) Shape marker [10]. (h) Marker optimization [11]. (i) Proposed technique. (j) Proposed technique with contour adjustment using the elliptical model.
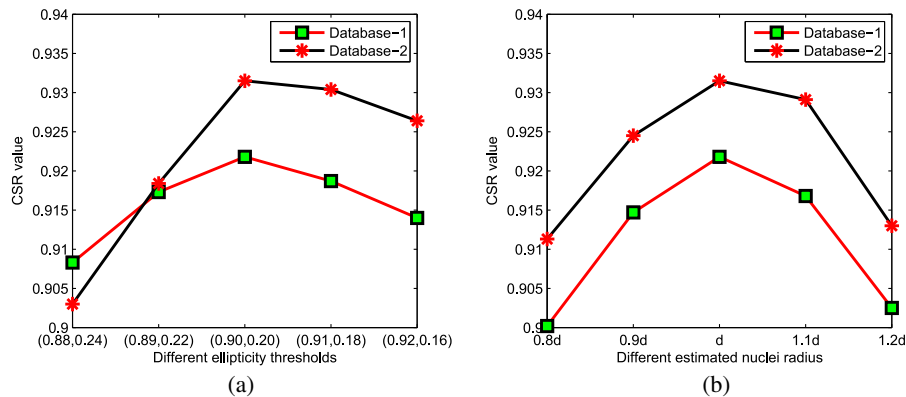

Fig. 13. Sensitivity of parameters on the nuclei segmentation performance. (a) CSR value with different ellipticity thresholds. (b) CSR value with different estimated nuclei radius.

Our seed detection technique is initially motivated by the SPV algorithm [16]. However, several improvements greatly reduce the computation complexity of the voting algorithm. First, an original color histopathological image is converted into a binary image and nuclei regions are shrunk by the erosion operation, and hence the proposed voting algorithm is able to select the potential voting regions from the eroded nuclei areas rather than from the whole image. Second, most isolated cell nuclei are efficiently detected by the ellipse descriptor analysis and avoid the unnecessary seed detection by the voting algorithm. To further show the efficiency of each module for the proposed technique, let us denote the first module (initial

segmentation) as the IS, the second module (ellipse descriptor analysis) as the EDA, the third module (seed detection) as the SD and the fourth module (nuclei segmentation) as the NS. Table IV shows the average run time required by the IS, IS+EDA, IS+EDA+SD, and IS+EDA+SD+NS (overall proposed technique), respectively. Note that $\bar{t}_1$ is calculated from database-1, while $\bar{t}_2$ is calculated from database-2. As observed in Table IV, the IS module takes around 10% of the total time, while the other three modules separately take around 30% of the total time. Overall, the proposed technique is time efficient due to the low complexity of the improved seed detection algorithm.

TABLE IV
THE AVERAGE RUN TIME FOR EACH MODULE OF THE PROPOSED TECHNIQUE (IS+EDA+SD+NS)[a]

Average Run Time	IS(s)	IS+EDA(s)	IS+EDA+SD(s)	IS+EDA+SD+NS(s)
$\bar{t}_1$	0.3	1.7	3.2	4.4
$\bar{t}_2$	0.2	0.8	1.5	2.1

[a]IS: Initial Segmentation. EDA: Ellipse Descriptor Analysis. SD: Seed Detection. NS: Nuclei Segmentation.

V. CONCLUSION

This paper presents an efficient computer-aided technique for segmentation of cell nuclei in the skin histopathological images. The proposed technique first extracts the candidate nuclei regions using an adaptive threshold technique, and then separates ellipse-like isolated nuclei using two ellipticity parameters. The seeds of clustered nuclei and nuclei with irregular shapes are detected by an improved voting algorithm. Finally, the undivided nuclei regions are segmented by the marked watershed algorithm with contours adjusted by the ellipsoidal model. The evaluation on 114 skin histopathological image patches shows that the proposed technique performs better than the existing methods and provides a correct segmentation rate of over 90%.

ACKNOWLEDGMENT

REFERENCES

[1] H. Fatakdawala, J. Xu, A. Basavanhally, G. Bhanot, S. Ganesan, M. Feldman, J. E. Tomaszewski, and A. Madabhushi, "Expectation–maximization-driven geodesic active contour with overlap resolution (emagacor): Application to lymphocyte segmentation on breast cancer histopathology," *IEEE Trans. Biomed. Eng.*, vol. 57, no. 7, pp. 1676–1689, Jul. 2010.

[2] C. Lu, M. Mahmood, N. Jha, and M. Mandal, "Automated segmentation of the melanocytes in skin histopathological images," *IEEE J. Biomed. Health Informat.*, vol. 17, no. 2, pp. 284–296, Mar. 2013.

[3] C. Lu, M. Mahmood, N. Jha, and M. Mandal, "A robust automatic nuclei segmentation technique for quantitative histopathological image analysis," *Anal. Quant. Cytol. Histol.*, vol. 34, pp. 296–308, 2012.

[4] S. M. Ismail, A. B. Colclough, J. S. Dinnen, D. Eakins, D. M. D. Evans, E. Gradwell, J. P. O.'Sullivan, J. M. Summerell, and R. G. Newcombe, "Observer variation in histopathological diagnosis and grading of cervical intraepithelial neoplasia," *Brit. Med. J.*, vol. 298, no. 6675, p. 707, 1989.

[5] T. Krenacs, I. Zsakovics, T. Micsik, L. Fonyad, S. V. Varga, L. Ficsor, G. Kiszler, and B. Molnar, "Digital microscopy: The upcoming revolution in histopathology teaching, diagnostics, research and quality assurance," *Microsc.: Sci., Technol., Appl. Edu.*, vol. 2, pp. 965–977, 2010.

[6] R. Guo and S. Pandit, "Automatic threshold selection based on histogram modes and a discriminant criterion," *Mach. Vis. Appl.*, vol. 10, no. 5–6, pp. 331–338, 1998.

[7] N. Otsu, "A threshold selection method from gray-level histograms," *IEEE Trans. Syst., Man, Cybern.*, vol. 9, no. 1, pp. 62–66, Jan. 1979.

[8] L. Vincent and P. Soille, "Watersheds in digital spaces: An efficient algorithm based on immersion simulations," *IEEE Trans. Pattern Anal. Mach. Intell.*, vol. 13, no. 6, pp. 583–598, Jun. 1991.

[9] X. Yang, H. Li, and X. Zhou, "Nuclei segmentation using marker-controlled watershed, tracking using mean-shift, and kalman filter in time-lapse microscopy," *IEEE Trans. Circuits Syst.*, vol. 53, no. 11, pp. 2405–2414, Nov. 2006.

[10] J. Cheng and J. C. Rajapakse, "Segmentation of clustered nuclei with shape markers and marking function," *IEEE Trans. Biomed. Eng.*, vol. 56, no. 3, pp. 741–748, Mar. 2009.

[11] C. Jung and C. Kim, "Segmenting clustered nuclei using h-minima transform-based marker extraction and contour parameterization," *IEEE Trans. Biomed. Eng.*, vol. 57, no. 10, pp. 2600–2604, Oct. 2010.

[12] Y. Al-Kofahi, W. Lassoued, W. Lee, and B. Roysam, "Improved automatic detection and segmentation of cell nuclei in histopathology images," *IEEE Trans. Biomed. Eng.*, vol. 57, no. 4, pp. 841–852, Apr. 2010.

[13] O. Schmitt and M. Hasse, "Morphological multiscale decomposition of connected regions with emphasis on cell clusters," *Comput. Vis. Image Understanding*, vol. 113, no. 2, pp. 188–201, 2009.

[14] H. Wang, H. Zhang, and N. Ray, "Clump splitting via bottleneck detection and shape classification," *Pattern Recog.*, vol. 45, no. 7, pp. 2780–2787, 2012.

[15] B. Parvin, Q. Yang, J. Han, H. Chang, B. Rydberg, and M. H. Barcellos-Hoff, "Iterative voting for inference of structural saliency and characterization of subcellular events," *IEEE Trans. Image Process.*, vol. 16, no. 3, pp. 615–623, Mar. 2007.

[16] X. Qi, F. Xing, D. J. Foran, and L. Yang, "Robust segmentation of overlapping cells in histopathology specimens using parallel seed detection and repulsive level set," *IEEE Trans. Biomed. Eng.*, vol. 59, no. 3, pp. 754–765, Mar. 2012.

[17] P. Yan, X. Zhou, M. Shah, and S. T. Wong, "Automatic segmentation of high-throughput rnai fluorescent cellular images," *IEEE Trans. Inf. Technol. Biomed.*, vol. 12, no. 1, pp. 109–117, Jan. 2008.

[18] M. Plissiti and C. Nikou, "Overlapping cell nuclei segmentation using a spatially adaptive active physical model," *IEEE Trans. Image Process.*, vol. 21, no. 11, pp. 4568–4580, Nov. 2012.

[19] D. Comaniciu and P. Meer, "Mean shift: A robust approach toward feature space analysis," *IEEE Trans. Pattern Anal. Mach. Intell.*, vol. 24, no. 5, pp. 603–619, May 2002.

[20] T. F. Chan and L. A. Vese, "Active contours without edges," *IEEE Trans. Image Process.*, vol. 10, no. 2, pp. 266–277, Feb. 2001.

[21] T. F. Chan, B. Y. Sandberg, and L. A. Vese, "Active contours without edges for vector-valued images," *J. Visual Commun. Image Representation*, vol. 11, no. 2, pp. 130–141, 2000.

[22] S. T. Acton and N. Ray, *Biomedical Image Analysis: Segmentation*. San Rafael, CA, USA: Morgan & Claypool Publishers, 2009.

[23] R. Gonzalez and R. Woods, *Digital Image Processing*, 3rd ed. Englewood Cliffs, NJ, USA: Prentice Hall, 2008.

[24] A. Fitzgibbon, M. Pilu, and R. B. Fisher, "Direct least square fitting of ellipses," *IEEE Trans. Pattern Anal. Mach. Intell.*, vol. 21, no. 5, pp. 476–480, May 1999.

Hongming Xu received the B.Sc. and M.Sc. degrees in computer engineering from Information Engineering College, Northwest A&F University, Shaanxi, China, in 2009 and 2012, respectively. He is currently working toward the Ph.D. degree in electrical engineering in the Multimedia Computing and Communication Lab, Department of Electrical Engineering, University of Alberta, Edmonton, AB, Canada.

His research interests include medical image analysis, pattern recognition, and computer vision.

Mr. Xu is the recipient of the Chinese Scholarship Council for his Ph.D. studies.

Cheng Lu (S'11) received the B.Sc. and M.Sc. degrees in computer engineering from Information Engineering College, Northwest A&F University, Shaanxi, China, in 2006 and 2008, respectively. He received the Ph.D. degree in electrical and computer engineering in University of Alberta, Edmonton, AB, Canada, in 2013.

He is now working in Shaanxi Normal University, Xi'an, China. His research interests include computer vision, medical image analysis, pattern recognition, and super resolution imaging. He has published several papers in leading international journals and conferences.

Mrinal Mandal (SM'03) received the B.E. degree in electronics and communication engineering from the National Institute of Technology, Durgapur, India, in 1987, the M.E. degree in electronics and communication engineering from the Bengal Engineering and Science University, India in 1989, and the M.A.Sc. and Ph.D. degrees in electrical and computer engineering from the University of Ottawa, Canada, in 1995 and 1998, respectively.

He is currently a Full Professor and Associate Chair with the Department of Electrical and Computer Engineering and is the Director of the Multimedia Computing and Communications Laboratory at the University of Alberta, Edmonton, AB, Canada. He has authored the book *Multimedia Signals and Systems* (Boston, MA, USA: Kluwer Academic), and coauthored the book *Continuous and Discrete Time Signals and Systems* (Cambridge, U.K.: Cambridge University Press). His current research interests include multimedia, image, and video processing, multimedia communications, and medical image analysis. He has published over 140 papers in refereed journals and conferences, and has a US patent on lifting wavelet transform architecture. He has been the Principal Investigator of projects funded by Canadian Networks of Centers of Excellence such as CITR and MICRONET, and is currently the Principal Investigator of a project funded by the NSERC.

Dr. Mandal was a recipient of Canadian Commonwealth Fellowship from 1993 to 1998, and the Humboldt Research Fellowship from 2005 to 2006 at Technical University of Berlin, Berlin, Germany.